Journal of ELECTRONIC MATERIALS, Vol. 47, No. 8, 2018
https://doi.org/10.1007/s11664-018-6245-2
© 2018 The Minerals, Metals & Materials Society

TOPICAL COLLECTION: 18TH INTERNATIONAL CONFERENCE ON II-VI COMPOUNDS

Effect of Intense Optical Excitation on Internal Electric Field Evolution in CdTe Gamma-Ray Detectors

K. SUZUKI,[1,3] Y. ICHINOHE,[1] and S. SETO[2]

1.—Hokkaido University of Science, Maeda 7-15, Teine Sapporo 006-8585, Japan. 2.—National Institute of Technology, Ishikawa College, Tsubata, Ishikawa 929-0392, Japan. 3.—e-mail: suzukik@hus.ac.jp

The time-of-flight (TOF) transient currents in radiation detectors made of CdTe and $Cd_{0.9}Zn_{0.1}Te$ (CZT) have been measured at several optical excitation intensities to investigate the effect of drifting carriers on the internal field. Both detectors show so-called space-charge-perturbed (SCP) current under intense optical excitation. A Monte Carlo (MC) simulation combined with an iterative solution of Poisson's equation is used to reproduce the observed currents under several bias voltages and excitation intensities. The SCP theory describes well the transient current in the CZT detector, whereas injection of holes from the anode and a corresponding reduction of the electron lifetime are further required to describe that in the CdTe detector. We visualize the temporal changes in the charge distribution and internal electric field profiles of both detectors.

Key words: Time of flight, space-charge perturbation, radiation detector, Monte Carlo simulation, CZT

INTRODUCTION

CdTe and $Cd_{1-x}Zn_xTe$ (CZT) are the most promising materials for room-temperature x- and gamma-ray detectors, owing to their high resistivity and good transport properties. Attempts to use these pulse-mode detectors for fast-scanning, high-flux x-ray applications such as computed tomography have been reported recently.[1] However, polarization at high x-ray fluxes (on the order of 10^8 counts mm^{-2} s^{-1}), which degrades the spectroscopic performance and detection efficiency, has been recognized and become a focus of interest. It is reported that, under such intense irradiation, semiconducting radiation detectors with low hole mobility suffer from a buildup of positive space charge that ultimately collapses the electric field and results in catastrophic device failure.[2] Franc et al. investigated the effect of subgap photoexcitation on the change in the internal electric field by using the Pockels electrooptic effect in CZT detector materials. They reported that electrons trapped at energy levels of 0.7 eV and 0.9 eV and holes trapped at an energy level of 0.8 eV dominated the change in the electric field, leading to polarization of the detectors.[3] Cola and Farella[4] investigated charge transport under strong optical excitation using the Pockels effect in combination with a transient charge technique. They discussed the effect of space-charge buildup due to deep trapped carriers on the deformation of the internal electric field. However, because the acquisition time of the Pockels effect is on the order of 100 ms whereas the carrier transient time for electrons is usually less than 1 μs, it is not possible to evaluate the internal field modification owing to drifting of the carriers themselves. As a result, those investigations[3,4] focused on the deformation of the internal electric field due to the trapped and hence immobile charges. However, perturbation of the electric field due to the drifting charge itself, referred to as space-charge perturbation (SCP), occurs even at much lower excitation intensities. The SCP has long been known in insulating materials such as iodine and sulfur.[5,6] We recently reported a bias-induced

(Received November 3, 2017; accepted March 17, 2018; published online March 30, 2018)

polarization that would occur due to the change in the deep-level occupation for CdTe detectors.[7] However, no systematic investigations of the dynamic change in the internal electric field due to the electron drift for CdTe and CZT have been reported to date. We measured the electron transient currents of these detector materials under strong optical excitation using a time-of-flight (TOF) technique. The current waveforms were further analyzed using a Monte Carlo (MC) simulation combined with an iterative solution of Poisson's equation, including the mobile charge distribution at each simulation step.

EXPERIMENTAL PROCEDURES

The samples used for the measurements were Pt/CdTe/Pt ($4 \times 4 \times 1$ mm^3) from Acrorad and Au/$Cd_{0.9}Zn_{0.1}Te$/Au ($5 \times 5 \times 1$ mm^3) from eV PRODUCTS. Hereinafter, we denote these as the CdTe detector and CZT detector, respectively.

Transient current waveforms were measured using a standard TOF configuration with a nitrogen laser (λ = 337 nm) operating at repetition rate of 8 Hz and nominal pulse duration of 300 ps as excitation source. We controlled the excitation intensity by rotating a variable neutral-density (ND) filter. The maximum intensity I_0 of the laser measured at the sample position by using a pyroelectric power meter was about 4 μJ per pulse when the ND filter was set to 0°. Transient current signals from the sample were fed directly into a digital oscilloscope (Tektronix TDS 3052, 500 MHz, 5 GS/s, 9 bits) through a 50-Ω load resistor. This value of the load resistor together with the sample capacitance (1.5 pF for CdTe and 2.3 pF for CZT) ensures a time constant for current–voltage conversion of less than 0.1 ns, much shorter than the transit time of the carrier drift. A pulse bias of 100 μs was applied 30 μs before each laser excitation to avoid bias-induced polarization.[7] The beam size of the laser was controlled so that the edge of the sample surface was not illuminated. All measurements were conducted at room temperature. A detailed description of the experimental method is given in Ref. 8.

RESULTS AND DISCUSSION

Figure 1 shows the TOF current waveforms of electron drift in the CZT detector under different optical excitation intensities (solid lines) from $0.01I_0$ to I_0 at bias voltage of − 200 V applied on the incident surface. The charge Q at each measurements is estimated by integrating each transient current waveform. The transient current at Q = 9.8 pC with its transit time T_R of about 50 ns is a conventional TOF current in which the generated charge is much smaller than CV (460 pC), where C denotes the geometric capacitance of the CZT detector and V is the applied bias voltage (200 V). Hereinafter, we designate this condition as

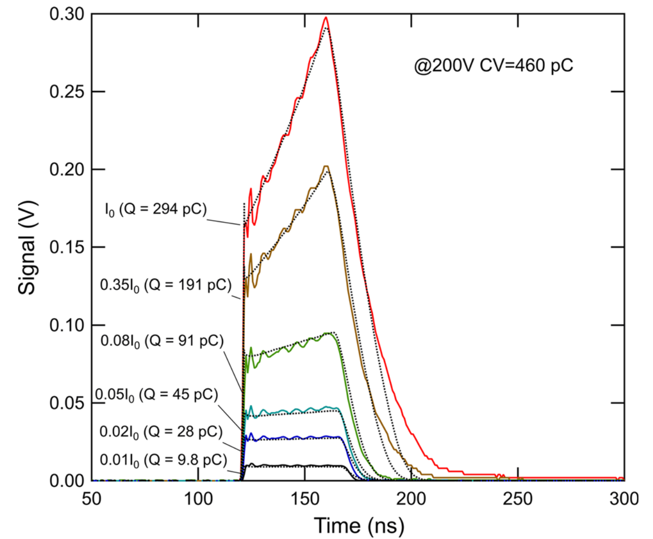

Fig. 1. Excitation intensity dependence of electron drift signals for the CZT sample (solid lines). Corresponding MC results are given by dotted lines.

space-charge-free (SCF) transport. In SCF transport, the drift velocity (v_d) determined from the transit time (T_R) increases linearly with the applied electric field strength. The drift mobility of the present sample estimated by the least-squares fit of v_d versus the applied electric field at room temperature was 960 cm^2/V-s. Measurements of transport properties such as drift mobility and trapping time under the SCF condition are widely used for various semiconductor materials such as a-Si:H[9] and organic semiconductors.[10]

The dotted line at the Q = 9.8 pC signal is the result of the MC simulation assuming a shallow trapping time τ^+ of 20 ns, shallow detrapping time τ_d of 1.8 ns, and deep trapping time τ_D^+ of 3.0 μs. Further, we assume scattering mobility of 1050 cm^2/V-s and a constant electric field strength calculated as the applied voltage divided by the sample thickness. It was reported in Ref. 11 that trapping and detrapping by a shallow level at 0.023 eV from the conduction band controls the drift mobility of high-resistivity CZT. The observed drift mobility is in line with the assumed scattering mobility if we take into account the reduction of the mobility by trapping–detrapping at the shallow trap. Since the material is fully compensated and high reverse bias field is applied, recombination of electrons with holes is unlikely during TOF measurements. Instead, deep trapping governs the charge collection efficiency. Possible candidates for the electron trap located at 0.7 eV and 0.9 eV from the conduction band are reported in Ref. 3 for a CZT detector with electron mobility–lifetime product of 1.5×10^{-3} cm^2/V-s. Details of this MC calculation are given in Ref. 8.

As shown in Fig. 1, although the applied bias voltage was kept constant at − 200 V, the transient

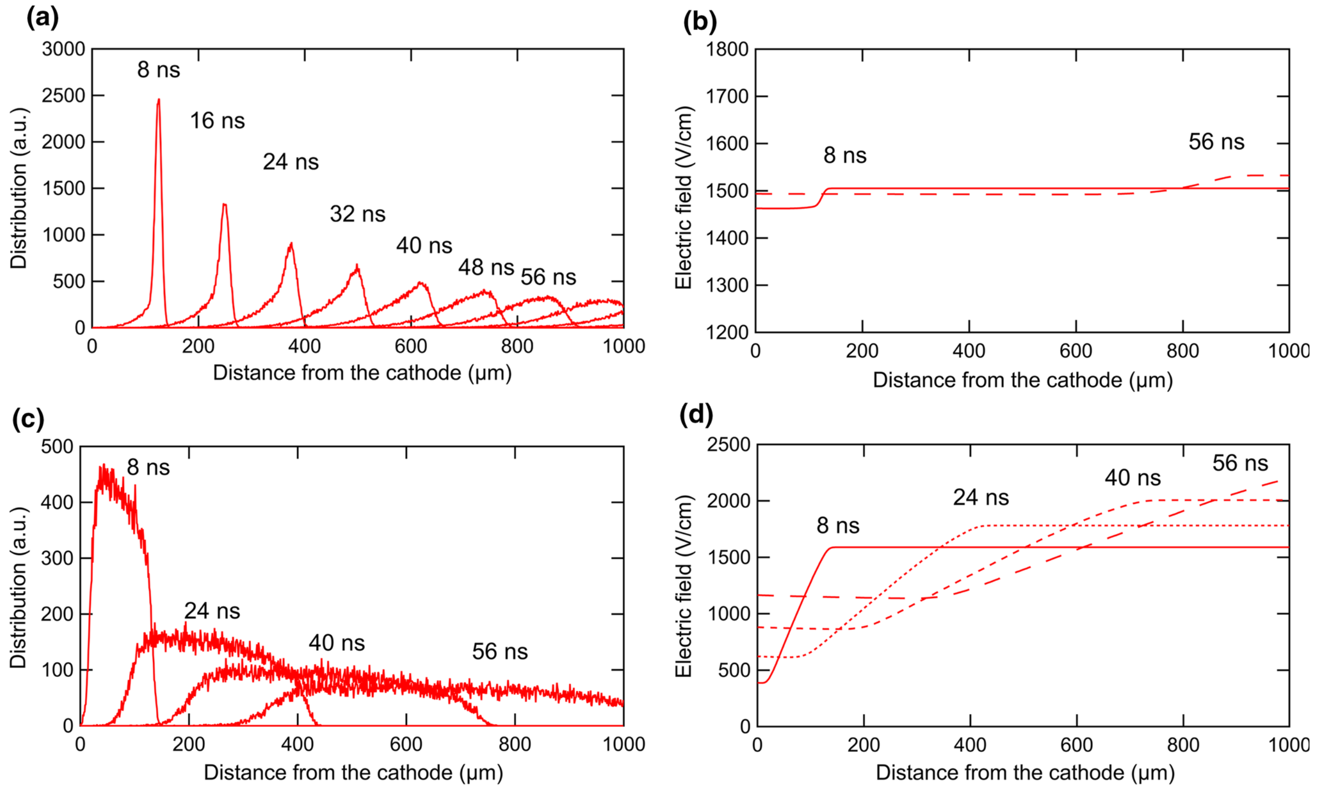

Fig. 2. (a) Charge distribution and (b) electric field evolution under the SCF condition. Charge distribution (c) and electric field evolution (d) under the SCP condition at $\beta' = 1.4$. Each sampling time in the MC simulation is indicated in the figures.

time increased with increasing excitation intensity owing to a long tail. Furthermore, the plateau observed at lower excitation intensities, which indicates a constant drift velocity, shows a rapid increase with increasing excitation intensity. Finally, a cusp appears at about $t \approx 0.7T_{\mathrm{R}}$ for the higher-excitation-intensity waveforms. Here, T_{R} is the carrier transit time for the $Q = 9.8$ pC signal. This deformation of the current waveforms is obviously due to perturbation of the internal electric field by the drifting carriers themselves. As previously stated, similar changes in the transient currents were reported in insulating materials under intense optical excitation.[5,6] The cusp indicates the arrival of the front edge of the charge distribution at the counterelectrode, and the corresponding time is defined as T_1 ($\approx 0.7T_{\mathrm{R}}$).[12] Namely, under high excitation, the internal electric field is no longer a constant, but rather increases with increasing distance from the cathode. The SCP state is characterized by β, which is defined as[12]

$$\beta = \frac{C_{\mathrm{s}}V}{Q_0}, \tag{1}$$

where C_{s} is the geometrical capacitance of the sample, V is the applied voltage, and Q_0 is the charge generated at the surface. Experimentally, however, it is not possible to measure the generated charge at $t = 0$; instead, we estimate β from the collected charge Q, provided that $\tau_{\mathrm{D}}^{+} \gg T_{\mathrm{R}}$. Hereinafter, we designate this value as β'.

Theoretical treatment of carrier transport under the SCP condition has only been given for very limited cases, such as trapping but no detrapping from a deep state.[12] However, the carriers in these detector materials suffer from frequent trapping and detrapping as they drift to the counterelectrode. Therefore, another theoretical treatment that allows arbitrary trapping–detrapping events is required to understand the experimental results for these detector materials. For this purpose, we solved Poisson's equation including the mobile charge distribution as well as the fixed charge distribution at each MC step. The dotted lines for the higher-excitation-intensity curves are the results of such calculations in which the transport parameters are the same as those in the SCF case, but the initial charge density is increased. Although a slight discrepancy is recognized for the tail region of the transient currents at 191 pC and 294 pC, probably due to the slight changes in the trapping parameters, the overall agreement between the experimental and MC results indicates the appropriateness of our simulation model. Therefore, it is worth discussing the charge distribution and electric field evolution derived from the simulation.

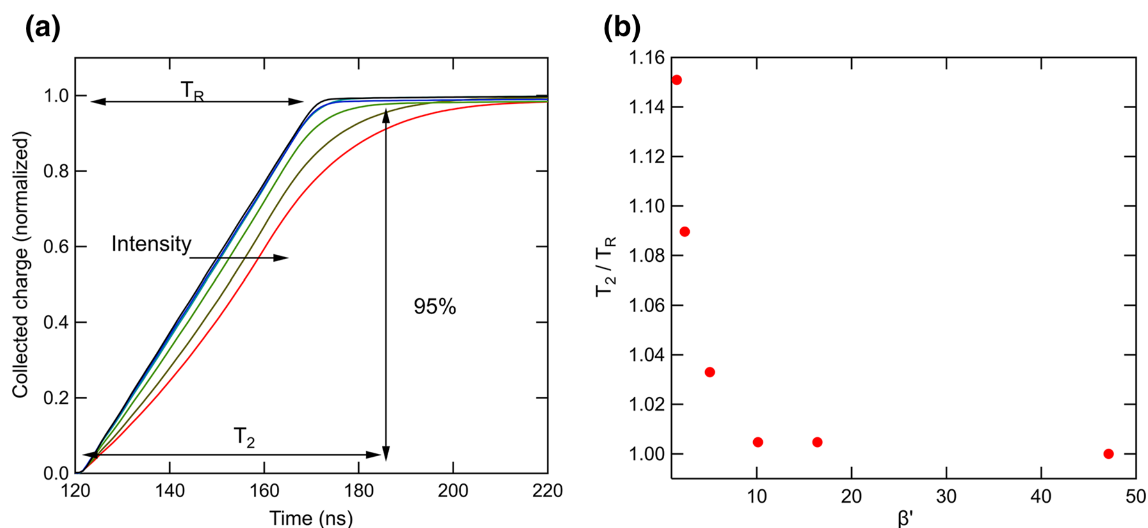

Fig. 3. (a) Time integral of transient currents at different excitation intensities from $0.01I_0$ to I_0 for CZT. (b) Each signal is normalized by the saturation value. T_2 is defined as 95% of the saturation value. T_2/T_R versus β'. Both (a) and (b) show the results at a bias voltage of − 200 V.

Figure 2a shows the calculated charge distribution under the SCF condition every 8 ns after charge generation at the cathode (t = 0) for bias voltage of − 150 V. In principle, the transport is described as nondispersive. However, a long tail at the trailing edge, due mainly to shallow trapping and detrapping, is remarkable. The corresponding electric field profiles at t = 8 ns and 56 ns are shown in Fig. 2b. A step corresponding to the movement of the front edge of the charge distribution from the cathode to the anode is identified. Therefore, strictly speaking, the electric field is perturbed by carrier drift even under the so-called SCF condition. This difference in the electric field strength on each side of the distribution is an additional reason for the long tail at the trailing edge of the charge distribution shown in Fig. 2a. Figure 2c shows the charge distribution under the SCP condition at bias voltage of − 150 V, which corresponds to β' = 1.4. Because the high-density electron distribution screens the externally applied field, the internal electric fields on each side of the charge distribution show significant differences (see Fig. 2d). This further broadens the charge distribution with time evolution owing to dispersion of the drift velocity. As a result, the distribution extends over nearly the entire sample length for $t \geq 56$ ns.

Obviously, this broadened distribution extends the full collection time of the charges. Figure 3a shows the time integral of the transient current at each excitation intensity. For lower excitation, a distinct transient time T_R is defined, whereas the time required for full collection increases with increasing excitation intensity. If we define the arrival of the rear edge of the charge distribution, T_2, as 95% collection, the collection time increases to about 115% for the transit time at our highest excitation intensity, which corresponds to β' = 1.4 (see Fig. 3b). This may be partly responsible for the delayed temporal response of the detector reported under high-flux x-ray irradiation.[1] It should be noted, however, that the absorption length and hence the generation region as well as the number of electron–hole pairs generated by the x-ray flux and the ultraviolet (UV) photon is very much different. The absorption length of the UV photon from the nitrogen laser is at most 1.0 μm from the incident surface. Since the photoexcitation takes place in an area of 3 mm × 3 mm, the maximum charge density of the present study is about 100 μC/cm^3. On the other hand, although the penetration depth of the x-ray depends on the target metal and the acceleration voltage used for its generation, the relevant interaction depth for high-flux polarization is reported to be around 100 μm.[13] This results in a charge density of about 4.6 mC/cm^3. Further, the laser excitation lasts less than 1 ns for the TOF measurements, while the samples are under continuous irradiation by the x-ray for the case of high-flux polarization.

The solid lines in Fig. 4 show the bias dependence of the transient current under the SCF ($0.01I_0$) and SCP (I_0) conditions for the CdTe sample at bias voltages of − 100 V to − 300 V. The transient currents under the SCF condition in principle show the same tendency as those of the CZT sample except for the roundness of the trailing edge. The drift velocity as estimated from the transit time increases linearly with increasing electric field, as shown in the inset of Fig. 4a. A drift mobility of

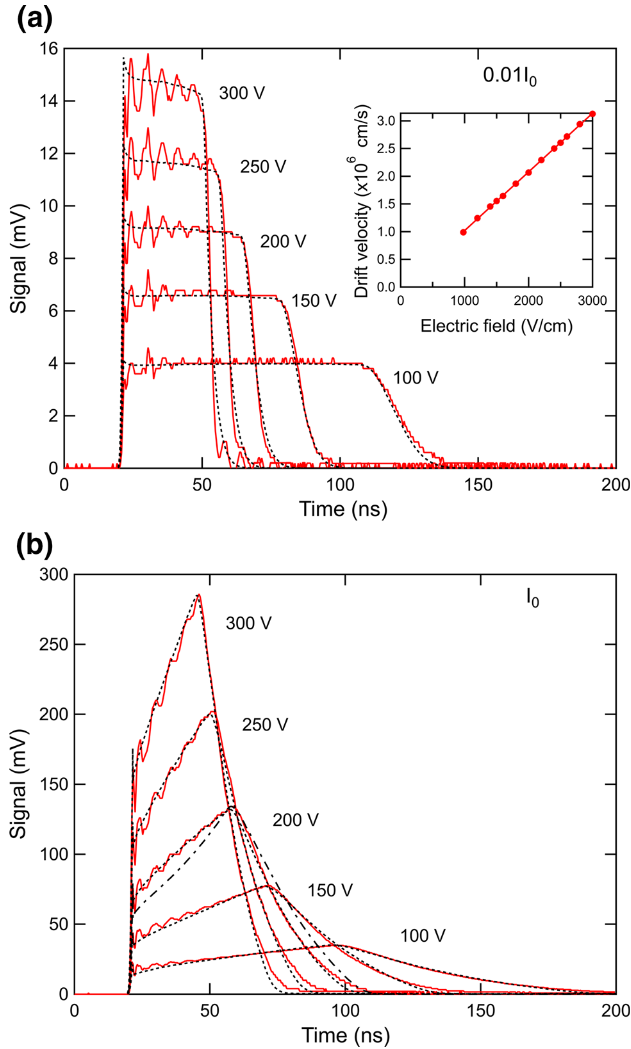

Fig. 4. Bias dependence of TOF signal for CdTe sample under (a) SCF at $0.01I_0$ and (b) SCP at I_0 conditions (solid lines). Dotted lines are results of MC simulation including (a) hole injection from the anode and (b) hole injection and reduction of the electron lifetime. The dash-dotted line at − 200 V in (b) is a model without injection or lifetime reduction, similar to that applied for CZT. The electric field dependence of the drift velocity at SCF condition is shown in the inset of (a). A drift mobility of 1058 cm^2/V-s is determined from the slope.

1058 cm^2/V-s is thus obtained from the slope. On the other hand, those for the SCP condition are notably different from those of the CZT sample. Namely, until T_1, the current shows a concave downward increase. Therefore, as shown by the dash-dotted line in Fig. 4b at − 200 V, it is not possible to reproduce the transient current of the CdTe sample under the SCP condition, only by the simple SCP model that works well for the CZT sample. Because of the small difference in the work functions of CdTe and Pt, hole injection is reported for Ohmic-type CdTe detectors.[14] Therefore, to calculate Poisson's equation, we include a positive space charge distribution $N^+(x)$ resulting from trapping of injected holes from the anode to deep levels, as shown in Eq. 2.

$$N^+(x) = N_d \exp\{-(d-x)/d_{inj}\}, \quad (2)$$

where d is the sample thickness, N_d is the charge injected at the anode ($x = d$), and d_{inj} is a characteristic length that determines the positive space-charge profile. In Ref. 14, the hole injection is reported to be on the order of 10^{11} cm^{-3} at 80 V. We thus started from this value to adjust d_{inj} as well as N_d to obtain the best fit to the experimental waveforms. The dotted lines in Fig. 4a are the results of a simulation that included injection of holes from the anode with a constant d_{inj} = 700 μm and a slightly bias-dependent N_d from 0.5×10^{10} cm^{-3} at − 100 V to 3×10^{10} cm^{-3} at − 300 V. Since shallow-trap-controlled transport, similar to that of CZT, was reported in CdTe,[11] a single set of trapping parameters, viz. τ^+ = 20 ns, τ_d = 1.5 ns, and τ_D^+ = 2.7 μs, was assumed for these simulations. An electron trap located at 0.81 eV below the conduction band with capture cross-section of 10^{-15} cm^2[15] may be responsible for the deep trapping time constant τ_D^+. However, for SCP transport, we further assume a reduction of the electron lifetime τ_D^+, since there is a considerable density of generated electrons as well as positive space charges that are injected and successively trapped. A possible candidate for such a hole trap is reported in Ref. 15 at 0.86 eV above the valence band with capture cross-section of 2×10^{-16} cm^2. The dotted lines in Fig. 4b are the results of simulation that also include the reduced electron lifetime. We assume a lifetime of 0.17 μs at bias voltage of − 300 V, which changes to 0.35 μs at bias voltage of − 100 V, as it would depend on the positive space-charge density. As shown in the figure, very good agreement with experimental results is obtained by including this reduction of the lifetime.

Figure 5a shows the evolution of the charge distribution derived from the proposed model for the SCF condition at 8-ns intervals after charge generation. The evolution of the distribution is qualitatively similar to that of the CZT sample. However, in Fig. 5b, a concave downward profile for the electric field is observed owing to the injection of holes from the anode.

As shown in Fig. 5c, the charge distribution for SCP transport (β' = 2.4) adheres to the cathode at the beginning of the drift period owing to the nearly zero electric field in the early stage of drifting as shown in Fig. 5d. Namely, the distortion is much more severe than that of the CZT sample at β' = 1.4.

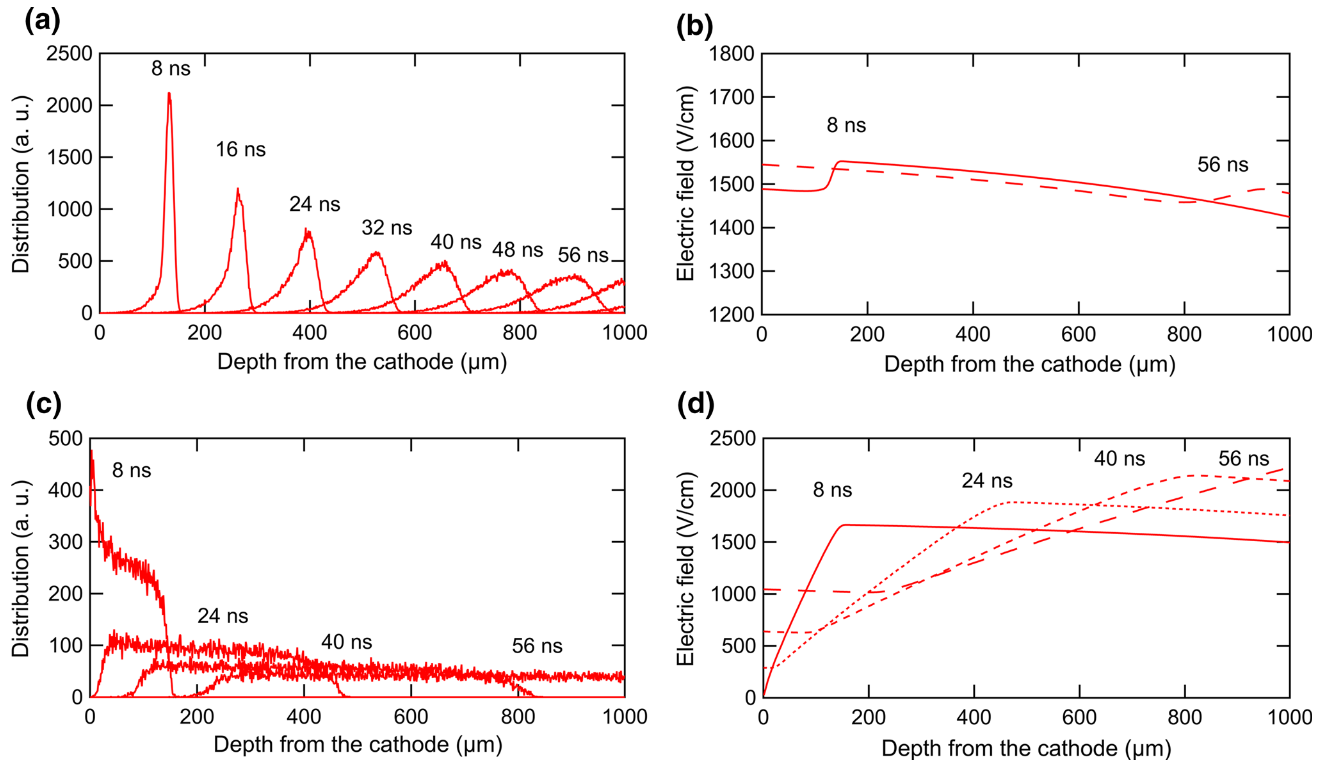

Fig. 5. (a) Charge distribution and (b) electric field evolution under SCF condition. (c) Charge distribution and (d) electric field evolution under SCP condition at $\beta' = 2.2$. Each delay time relative to excitation is indicated in the figures.

Obviously, the replacement of β (defined as the generated charge at $t = 0$) by β' (the collected charge at $t = T_R$) is inappropriate for such a short electron lifetime.

CONCLUSIONS

The effect of intense optical excitation on the TOF current waveforms of CdTe and CZT detectors was investigated. An MC simulation with the solution of Poisson's equation taking into account the mobile charge distribution successfully reproduced the charge distribution and evolution of the internal field as well as the transient current under the SCP condition for the CZT detector. However, for CdTe transport, injection of holes from the anode clearly plays a significant role in determining the transient current under the SCF condition. As a result, although it is negligibly small, the internal electric field shows a slightly concave downward profile even under the so-called SCF condition. Further, a reduction of electron lifetime was applied to successfully reproduce the concave downward increase of the transient current under the SCP condition. It was reported in Ref. 4 without showing the transient currents that, under strong optical injection, an Ohmic detector does not exhibit the expected behavior, such as the cusp-like peak associated with the space-charge-limited transient model. However, the present results clearly demonstrate that the internal electric field modification due to mobile charges, namely space-charge perturbation, occurs at a much lower excitation intensity than reported in Ref. 4.

REFERENCES

1. M. Prokesch, D.S. Bale, and C. Szeles, *IEEE Trans. Nucl. Sci.* 57, 2397 (2010).
2. M. Strassburg, Ch Schroeter, and P. Hackenschmied, *J. Instrum.* 6, C01055 (2011).
3. J. Franc, V. Dedic, J. Zazvorka, M. Hakl, R. Grill, and P.J. Sellin, *J. Phys. D Appl. Phys.* 46, 235306 (2013).
4. A. Cola and I. Farella, *Appl. Phys. Lett.* 105, 203501 (2014).
5. D.J. Gibbons and A.C. Papadakis, *J. Phys. Chem. Solids* 29, 115 (1968).
6. A. Many, M. Simhony, S.Z. Weisz, and J. Levinson, *J. Phys. Chem. Solids* 22, 285 (1961).
7. K. Suzuki, T. Sawada, and S. Seto, *Phys. Status Solidi C* 13, 656 (2016).
8. K. Suzuki, T. Sawada, and K. Imai, *IEEE Trans. Nucl. Sci.* 58, 1712 (2011).
9. W.E. Spear, *J. Non-Cryst. Solids* 1, 197 (1969).
10. T.J. Pundsack, N.O. Haugen, L.R. Johnstone, C.D. Frisbie, and R.L. Lidberg, *Appl. Phys. Lett.* 106, 113301 (2015).
11. K. Suzuki, S. Seto, T. Sawada, and K. Imai, *IEEE Trans. Nucl. Sci.* 49, 1287 (2002).
12. A.C. Papadakis, *J. Phys. Chem. Solids* 28, 641 (1967).
13. D.S. Bale and C. Szeles, *J. Appl. Phys.* 107, 114512 (2010).
14. I. Farella, G. Montagna, A.M. Mancini, and A. Cola, *IEEE Trans. Nucl. Sci.* 56, 1376 (2009).
15. R. Grill, E. Belas, J. Franc, M. Bugar, Š. Uxa, P. Moravec, and P. Hoschl, *IEEE Trans. Nucl. Sci.* 58, 3172 (2011).